Supplementary Material for

"Vector demography, dispersal, and the spread of disease: Experimental epidemics under elevated resource supply"

Alexander T. Strauss[1,2] (straussa@umn.edu), Jeremiah A. Henning[1,3] (jhenning@umn.edu), Anita Porath-Krause[1] (aporathk@umn.edu), Ashley L. Asmus[1] (aasmus@umn.edu), Allison K. Shaw[1] (ashaw@umn.edu), Elizabeth T. Borer[1] (borer@umn.edu), and Eric W. Seabloom[1] (seabloom@umn.edu)

[1]Department of Ecology, Evolution, and Behavior, University of Minnesota, St. Paul, MN, USA

[2]Current affiliation: Odum School of Ecology, University of Georgia, Athens, GA, USA

[3]Current affiliation: Department of Biology, University of South Alabama, Mobile, AL, USA

Corresponding author: Alex Strauss, straussa@uga.edu

APPENDIX

In this appendix, we present supplementary methods and results. First, we provide additional details about the experiment. We report the formulas for nutrient solutions (Table S1), describe the maintenance of aphid and virus cultures in the lab, and describe a simple experiment that shows that the dispersal of aphids away from an initial piece of host tissue does not depend on the number of hours that they were attached to it (Fig. S1). We also graphically depict our spatial sampling regime for the arenas (Fig. S2) and describe details of our standard laboratory protocol for diagnosing plant infections.

Next, we provide additional details about the models and model fitting. We show graphically that the *lagged dispersal* model converges onto the *non-spatial* model as dispersal

rate (*d*) increases (Fig. S3). We derive analytical equilibria for the *non-spatial* and *lagged dispersal* models, and approximate equilibria of the *traveling wave* models with simulations (Fig. S4). Then, we define the likelihood function used to fit the models to the data, and we confirm the performance of the model fitting machinery by testing it on simulated data with known underlying parameters (Fig. S5). We graphically show each spatial model fit to one treatment of the experiment, including the simplified *non-spatial* model (model 1F), the best overall *lagged dispersal* model (model 2A), and the analogous *travelling wave* model (model 2F; Fig. S6). We also report the fitted parameters for each of these models (Table S2). Finally, we plot likelihood surfaces for all pairwise combinations of the parameters *r*, *K*, and *d* in the best overall model (Fig. S7).

Nutrient solutions

We watered plants in the experiment with modified Hoagland's nutrient solutions (Hoagland and Arnon 1950). Concentrations of both nitrogen (as ammonium nitrate) and phosphorus (as monopotassium phosphate) corresponded to 0.1% (treatments with low resource supply; -R) or 5% dilutions (treatments with high resource supply; +R) of the original recipe. Concentrations of all micronutrients and macronutrients are tabulated below (Table S1).

Table S1. *Nutrient solutions.*

Compound	Formula	Concentration (µM)
potassium sulfate	K_2SO_4	1250
magnesium sulfate	$MgSO_4.7H_2O$	1000
calcium sulfate	$CaSO_4 \cdot 2H_2O$	2000
potassium chloride	KCl	25
boric acid	H_3BO_3	12.5
magnesium sulfate	$MnSO_4 \cdot H_2O$	1
zinc sulfate	$ZnSO_4 \cdot 7H_2O$	1
copper sulfate	$CuSO_4 \cdot 5H_2O$	0.25
molybdic acid	$H_2MoO_4 \cdot (H_2O)$	0.25
ferric sodium EDTA	NaFeEDDHA (6% Fe)	10
monopotassium phosphate	KH_2PO_4	1 or 50*
ammonium nitrate	NH_4NO_3	7.5 or 375*

* *depending on nutrient treatment: low (-R) or high (+R) resource supply*

Virus maintenance

The virus (CYDV-RPV) was originally isolated by the laboratory of Dr. Stewart Gray from cereal crops in New York state (Cornell University, Ithaca, NY). We have continuously maintained this strain of RPV by transferring ~25 viruliferous aphids (*R. padi*) to new cohorts of cultivated oats (*A. sativa*) every ~3 weeks since 2017. We maintained these cultures of plants, aphids, and viruses in a separate room from the experimental arenas, but under similar conditions (23°C; 16:8 light:dark; 2x 40 W cool white fluorescent bulbs). These plants were grown in Sunshine MVP potting soil (Sun Gro Horticulture) in 15 x 15 cm pots and watered twice per week with tap water. To obtain infected plant tissue for the experiment, we removed all aphids from several infected plants with 5-10 sprays (6-15 ml) of 1.6% dilute Fulfill insecticide

(Adama, USA). This pesticide prevents aphids from feeding for up to two months. It does not interfere with viral infections within host tissues, but it allows infected plants to grow for longer periods without being infested by aphids. Following standard laboratory procedure, we waited several months before harvesting this infected plant tissue for our experiment. This lag period ensured that aphids could feed again on the infected plant tissue and acquire the virus.

Dispersal of aphids away from initial host tissues

We used slightly different methods to add vectors to the experimental arenas with (+D) and without pathogens (-D), but this difference is unlikely to have biased our results. For treatments without the virus, we added the aphids to empty vials, starved them for two hours, added uninfected plant tissue, waited ~3 hours for the aphids to attach to the tissue, and then added the tissue and aphids to the center of their experimental arenas. We treated the infectious aphids very similarly, but waited 48 hours for them to attach to RPV-infected tissue and acquire the virus (Gray 2008) before adding them to their arenas. We were concerned that this slight difference in timing (3 versus 48 hours spent in the vial attached to the plant tissue) could have influenced the dispersal of aphids away from this initial tissue. Therefore, we conducted a simple complementary experiment.

This complementary experiment crossed the duration of time in the vial (3 or 48 hours) by presence of the virus in the plant tissue (healthy or infected with RPV). We replicated each combination of treatments 5 times, for a total of 20 trials. For each trial, we added 10 aphids to a vial, starved them for two hours, added plant tissue (either uninfected or infected with RPV), and allowed the aphids to attach and feed (either 3 or 48 hours). We then placed the tissue and aphids

on the center of a 15 x 15 cm piece of paper with sticky tape along the perimeter. We placed the paper on top of a moist Kimwipe and sealed the entire trial in a plastic container to maintain humidity. We checked the experiment daily and counted the aphids that remained on the plant tissue and the aphids that had dispersed. We used a linear model to test whether the cumulative proportion of dispersing aphids depended on the time since the plant tissue was placed on the paper (time since addition), the time that the aphids had remained attached to the plant tissue in the vial (3 or 48 hours), infection status of the plant tissue (healthy or infected with RPV), and two-way interactions between each treatment and the time since addition. The only significant effect was an increase in the cumulative proportion of dispersing aphids over time ($p < 1x10^{-12}$). All aphids in all treatments dispersed away from the initial plant tissue within two days. Neither time in the vial nor infection status altered this rate of dispersal (Fig S1). Thus, the difference in the number of hours that aphids spent in vials is unlikely to have biased results in the experimental arenas.

Fig. S1. *All aphids dispersed away from plant tissues within two days, and time in the vial did not affect this rate of dispersal.* The complementary experiment crossed time in the vial (upward triangles = 3 hours; downward triangles = 48 hours) with infection status of the plant tissue (open triangles = healthy; closed symbols = infected with RPV).

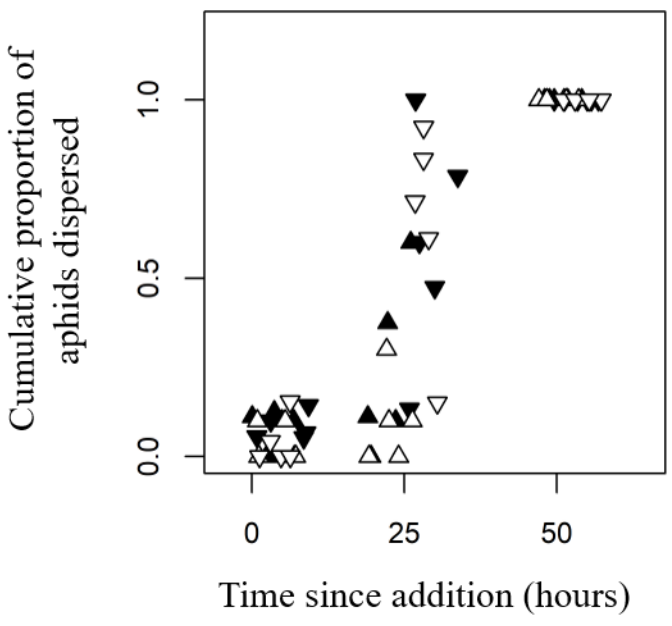

Graphical depiction of the sampling regime

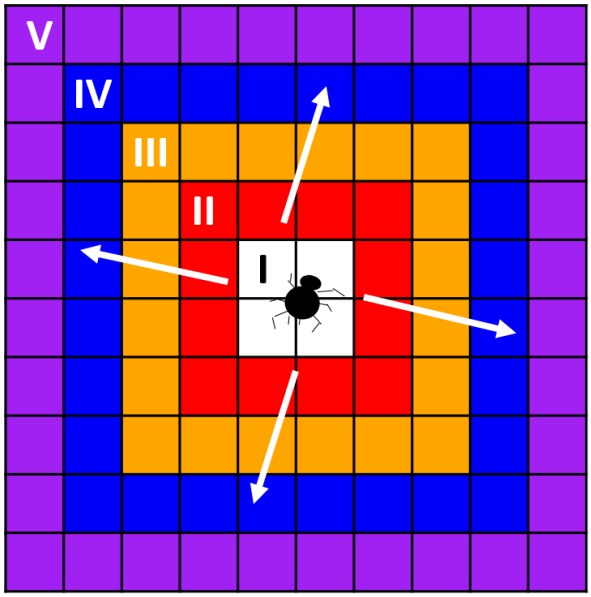

Fig. S2. *Hosts were sampled from randomized spatial gradients ranging from the centers of the arenas outward.* Aphids were added to the center of each arena (I). Each week, four hosts were sampled from each arena, with one host randomly selected from each of four concentric rings (labeled II, III, IV, and V) expanding outward from the center. No plants were sampled from the innermost four slots (I). Color and labeling scheme matches data plotted in Figs. 3 & S6.

Diagnosing infections from plant tissues

We diagnosed infections in plant hosts following standard laboratory procedures. In summary, we flash-froze plant tissues, extracting total RNA with TRIzol® Reagent (Invitrogen™) and chloroform, synthesized cDNA with generic primers, amplified virus cDNA with RPV-specific primers, and used gel electrophoresis to visually diagnose whether plants were infected.

We extracted total RNA following a standard laboratory protocol. Immediately after sampling, we cut 0.04-0.07g tissue from each plant (from the newest leaf, if possible) and flash-froze it in liquid nitrogen. Later, we cut these frozen tissue samples into 1-2 mm pieces, added them to microcentifuge tubes containing 500 µl TRIzol®, and pulverized them with steel BBs in

a bead beater at 10 second intervals until fully homogenized (Mini-Beadbeater-16 Biospec Products). Then we added 100 µl chloroform to the tubes, mixed by inverting (15 s), and cold-centrifuged (4 C, 7,000 g, 15 min). We transferred the aqueous phases to new tubes containing 100 µl isopropanol, mixed by inverting, and cold-centrifuged again (7,000 g, 10 min). Next, we discarded the supernatant, added 1 ml 75% ethanol, briefly vortexed our samples, cold-centrifuged for a third time (4 C, 7,000 g, 5 min), and discarded the supernatant. Finally, we allowed the pellets containing RNA to dry (minimum 30 min) before dissolving the pelleted RNA in 20 µl RNase-free water and freezing these total RNA samples for future use (-20 C).

We synthesized complementary DNA (cDNA) from the total RNA samples using reverse transcription polymerase chain reactions (RT-PCR). We mixed 4.5 µl of RNA solution from each sample and 0.5 µl of random hexamers (1ug/ul) and preheated these mixtures (70 C, 5 min) in a thermocycler (S1000^{TM} Thermal Cycler [Bio-Rad]). Each RT-PCR reaction (20 ul) contained 5 µl of this random hexamer/RNA mixture, 4 µl 5x Reaction Buffer (ImProm-II^{TM} Reverse Transcriptase [Promega]), 1.2 µl $MgCl_2$ (25mM), 1 µl dNTPs (10mM), 0.5 µl Recombinant RNasin® Ribonuclease Inhibitor (Promega; 40U/ul), 1 µl (ImProm-II^{TM} Reverse Transcriptase [Promega]), 7.3 µl RNase free water, and 0.034 µl T4 Gene 32 Protein (New England BioLabs). Thermocycler conditions for cDNA synthesis were 5 min at 25 C, 60 min at 45 C, and finally 15 min at 70 C.

Next, we amplified viral cDNA with RPV-specific primers via PCR. Each reaction (20 ul) included 2 µl 10x buffer, 2.8 µl $MgCl_2$ (25mM), 10.4 µl nanopure water, 0.8 µl each forward (5' - ATG TTG TAC CGC TTG ATC CAC - 3') and reverse (5' - CTG CGT TCT GAC AGC AGG - 3') primers (10 uM), 0.8 µl dNTPs (10 mM), 0.4 µl HotStarTaq® DNA Polymerase (Qiagen), and 0.068 µl T4 Gene 32 Protein (New England BioLabs). The thermocylcer program

included an initial heating phase (95 C, 15 min), a step-down phase (95 C [30 s], 59 C [30 s], and 72 C [60 s] with subsequent annealing iterations reduced from 59 C to 54 C in 1 C increments), and 29 cycles (95 C [30 s], 54 C [60 s], and 72 C [60 s]). Finally, we used gel electrophoresis to visually diagnose infections. We loaded the amplified DNA samples into 2.0% gel (UltraPure Agarose-1000, Thermo Fisher Scientific) mixed with SYBR Safe DNA Gel Stain (Invitrogen™) and visualized with Gel Doc™ EZ Imager (Bio Rad).

Convergence of the *lagged dispersal* and *non-spatial* models

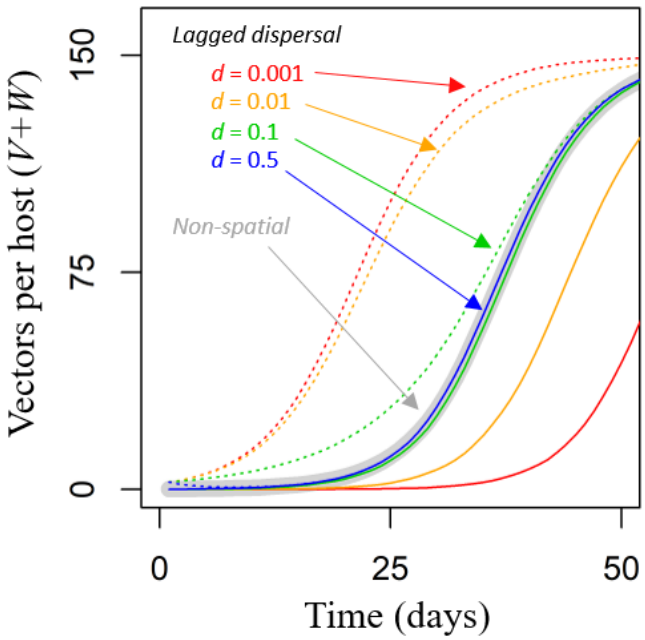

Figure S3. *The lagged dispersal model converges onto the non-spatial model as dispersal rates increase.* As dispersal rates increase (colored lines), differences in vector abundance between donor hosts (dashed lines) and receiver hosts (solid lines) become smaller. When dispersal rates are ~0.5 day^{-1} (blue lines) they become indistinguishable. At this point, the *lagged dispersal* model converges on the *non-spatial* model (thick gray line), because so much movement of vectors among hosts homogenizes spatial dynamics. Since we were not tracking the movement of individual aphids in our experiment, dispersal rates exceeding ~0.5 day^{-1} in the *lagged dispersal* model were indistinguishable and meaningless. Therefore, we set an upper limit of 0.5 on the estimation of the parameter d. Other parameters: K=150 vectors host^{-1}, r=0.2 day^{-1}, β_{VH}=0.001 hosts vector^{-1} day^{-1}, β_{VH}=0.68 arenas host^{-1} day^{-1}.

Equilibria of the models

In the *non-spatial* and *lagged dispersal* models, all hosts eventually become infected and all vectors reach their carrying capacity. Changes in the density of susceptible hosts (eq. 3) and infected hosts (eq. 4) both become zero when susceptible hosts are depleted (S_i=0). Thus, expressions for equilibrial densities (denoted with *) of susceptible (S) and infected hosts (I) are

$$S_i^* = 0 \qquad I_i^* = H_i \qquad \text{eq. S1}$$

where H_i is the total density of hosts in spatial class i ($H_i = S_i + I_i$). The equilibrial abundances of noninfectious (V) and infectious vectors per host (W) are slightly more complicated. Adding eqs. 1 & 2 creates an equation for the change in the abundance of total vectors per host

$$\frac{dX_i}{dt} = rX_i\left(1 - \frac{X_i}{K}\right) - dX_i + d(X_{m,i}) \qquad \text{eq. S2}$$

where X_i is the sum of noninfectious and infectious vectors ($X_i = V_i + W_i$ and $X_{m,i} = V_{m,i} + W_{m,i}$). Setting this equation to zero reveals a general expression for equilibrial vector abundance:

$$X_i^* = K + K\frac{d}{r}\left(\frac{X_{m,i}^*}{X_i^*} - 1\right) \qquad \text{eq. S3}$$

For the *non-spatial* model, $V_{m,1} = V_1$ and $W_{m,1} = W_1$ (eq. 5a-b in the main text). It follows that $X_{m,1}^* = X_1^*$ and consequently, the equilibrial abundance of vectors per host (eq. S3) collapses to:

$$X_1^* = K \qquad \text{eq. S4}$$

which unsurprisingly recapitulates simple (i.e., non-spatial) logistic growth.

For *lagged dispersal*, we set eq. S2 equal to zero for both donor (X_1) and receiver classes (X_2) simultaneously:

$$rX_1^*\left(1 - \frac{X_1^*}{K}\right) - dX_1^* + d(X_{m,1}^*) = 0 = rX_2^*\left(1 - \frac{X_2^*}{K}\right) - dX_2^* + d(X_{m,2}^*) \qquad \text{eq. S5}$$

Since the immigration terms are identical for donor and receiver classes, $dV^*_{m,1} = dV^*_{m,2}$ and $dW^*_{m,1} = dW^*_{m,2}$ (eq. 6a-b in the main text), it follows that

$$X^*_{m,1} = X^*_{m,2} = X^*_1 \frac{H_1}{H_1+H_2} + X^*_2 \frac{H_2}{H_1+H_2} \quad \text{eq. S6}$$

Substituting this equality into equation S5 makes it clear that an equilibrium exists when vectors on both donor and receiver hosts reach the same equilibrial carrying capacity, *K:*

$$X^*_1 = X^*_2 = K \quad \text{eq. S7}$$

Thus, equilibria of the *lagged dispersal* and *non-spatial* models are identical.

However, in the *travelling wave* model, extremely high dispersal rates can cause vectors to reach different equilibrial densities on different spatial classes of hosts. In extreme scenarios, hosts in earlier spatial classes can even remain uninfected. These effects arise if vectors emigrate out of the early spatial classes faster than they reproduce. These unique qualities of the *travelling wave* model are enabled by its reflecting boundary conditions and asymmetric dispersal (i.e., inner hosts receive fewer immigrants than outer hosts). We made these assumptions of reflecting boundaries, because they seemed most likely to capture spatial dynamics in the experiment. Because equilibria of the *travelling wave* model are less tractable than for the *non-spatial* and *lagged dispersal* models, we explore them with simulations (Fig. S4) rather than analytically.

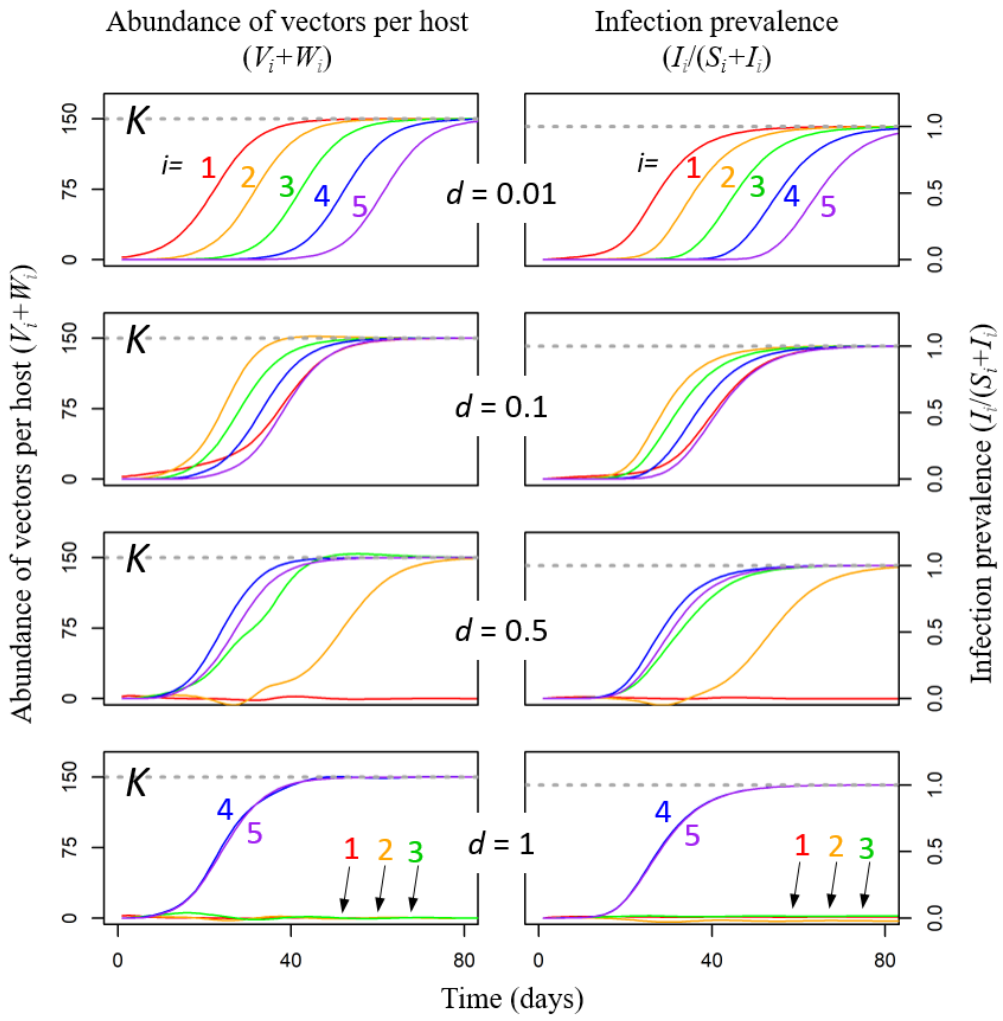

205

206 **Figure S4.** *Simulated equilibria of the travelling wave model.* With low dispersal rates (top row;
207 d=0.01 day^{-1}) vectors in each class (V_i+W_i; colored lines; labeled 1-5) approach the carrying
208 capacity K (gray dashed line) and all hosts become infected (infection prevalence [I_i/(S_i+I_i)]
209 approaching 1). With higher dispersal rates (d=0.1 day^{-1}; second row), the hosts and vectors
210 reach the same equilibria, but the first spatial class (i=1; red) reaches them more slowly. With
211 even higher dispersal rates (d=0.5 day^{-1}; third row), vector abundance and infection prevalence
212 of the first spatial class remains at zero. This effect cascades to the second and third classes with
213 even higher dispersal rates (d=1 day^{-1}; bottom row). These results make sense: Extremely high
214 dispersal rates and asymmetric movement due to reflecting boundaries cause vectors to leave the

early classes faster than they can reproduce. Other parameters: K=150 vectors host^{-1}, r=0.2 day^{-1}, β_{VH}=0.001 hosts vector^{-1} day^{-1}, β_{VH}=0.68 arenas host^{-1} day^{-1}. Travelling wave models fit to the experimental data had dispersal rates ranging from 0.09 – 0.44 day^{-1} (consistent with the second and third rows). These models fit the data very poorly (Table 3).

Model fitting

We used maximum likelihood to determine parameters of the dynamical models that best predicted the observed plant infections (assumed to follow a Bernoulli distribution) and aphid abundances (assumed to follow a negative binomial distribution). Starting conditions of the model simulations matched the experimental design (without disease: *non-spatial* V=0.1, W=0, S=100, I=0; *lagged dispersal* V_1=2.5, V_2=0, $W_{1\text{-}2}$=0, S_1=4, S_2=96, $I_{1\text{-}2}$=0; *travelling wave* V_1=2.5, $V_{2\text{-}5}$=0, $W_{1\text{-}5}$=0, S_1=4, S_2=12, S_3=20, S_4=28, S_5=36, $I_{1\text{-}5}$=0; with disease: swapping V_1 and W_1).

The probability mass function for a Bernoulli variable x is:

$$Bernoulli\ (x|p) = p^x(1-p)^{1-x} \qquad \text{eq. S8}$$

where p is the probability that x = 1, and 1-p is the probability that x = 0. We determined the probability of infection p for plant hosts with simulations of the dynamical models. We defined p as infection prevalence at a given spatial class of host (i) and time (t):

$$p_{i,t} = \frac{I_{i,t}}{S_{i,t}+I_{i,t}} \qquad \text{eq. S9}$$

We assumed that each observation was independent, for j = 1,...,J observations per spatial class (i = i_0,…n) per time (t = 1,…T). The indexing varied by model (*non-spatial:* n = 1, T = 8, J = 20; *lagged dispersal:* n = 2, T = 8, J = 20 in the receiver class i = 2; *travelling wave:* n = 5, T = 8, J =

5 in classes i = 2-5). The likelihood (L) of our joint infection data x, given parameters of the dynamical model, can therefore be written:

$$L(x) = \prod_{j=1}^{J} \prod_{i=i_0}^{n} \prod_{t=1}^{T} {p_{i,t}}^{x_{j,i,t}} (1 - p_{i,t})^{1 - x_{j,i,t}} \qquad \text{new eq. S10}$$

with the spatial class index starting at 1 for the non-spatial model (i_0=1) and 2 for the lagged dispersal and travelling wave models (i_0=2), since data were not collected from ring I (i.e., the centers) of the arenas.

Similarly, we assumed that the abundance of aphids per plant followed a negative binomial distribution. The probability mass function for a negative binomial variable y, following the 'alternative' parameterization with a mean and overdispersion parameter (Carpenter et al. 2015), is

$$Negative\ Binomomial\ (y|\mu, \theta) = \binom{y + \frac{1}{\theta} - 1}{y} \left(\frac{\mu}{\mu + \frac{1}{\theta}}\right)^{y} \left(\frac{\frac{1}{\theta}}{\mu + \frac{1}{\theta}}\right)^{\frac{1}{\theta}} \qquad \text{eq. S11}$$

where μ is the mean of the negative binomial distribution and θ controls its overdispersion relative to Poisson. The variance of a Poisson distribution equals its mean. This parameterization of the negative binomial distribution facilitates cases where variance exceeds the mean (i.e., cases of 'overdispersion'), which is common in ecological count data (Ver Hoef and Boveng 2007). The variance of this parameterization equals $\mu + \mu^2\theta$. If $\theta \sim 0$, this distribution converges to a Poisson (variance equals μ); if $\theta > 0$, the distribution is 'overdispersed', and the magnitude of its overdispersion is proportional to θ, weighted by the square of the mean μ. We determined the mean of the negative binomial distribution μ with simulations of the dynamical model, and defined it as the total number of aphids per host at a given spatial class (i) and time (t):

$$\mu_{i,t} = V_{i,t} + W_{i,t} \qquad \text{eq. S12}$$

We assumed that each observation of our aphid abundance data was independent, for $j = 1,...,J$ observations per spatial class ($i = i_0,\ldots n$) per time ($t = 1,\ldots T$). Therefore, the likelihood (L) of our joint aphid data y, given parameters of the dynamical model and the fitted overdispersion parameter θ, can be written:

$$L(y) = \prod_{j=1}^{J} \prod_{i=i_0}^{n} \prod_{t=1}^{T} \binom{y_{j,i,t}+\frac{1}{\theta}-1}{y_{j,i,t}} \left(\frac{\mu_{i,t}}{\mu_{i,t}+\frac{1}{\theta}}\right)^{y_{y,i,t}} \left(\frac{\frac{1}{\theta}}{\mu_{i,t}+\frac{1}{\theta}}\right)^{\frac{1}{\theta}} \quad \text{eq. S13}$$

with the spatial class index starting at 1 for the non-spatial model (i_0=1) and 2 for the lagged dispersal and travelling wave models (i_0=2). Finally, we assumed that the infection data and aphid data were independent to obtain an overall likelihood function:

$$L = L(x)L(y) \quad \text{eq. S14}$$

For computational tractability, we performed calculations on a log-transformed scale and therefore added the log-likelihoods instead of multiplying the untransformed likelihoods.

Performance of the model fitting machinery

We chose the optimizer "L-BFGS-B" for two reasons. First, the default optimizer in the package bbmle (method "Nelder-Mead") converged on different solutions when we started with different initial guesses for parameter values. In contrast, the optimizer "L-BFGS-B" proved to be highly consistent regardless of initial parameter guesses. Second, an optimizer with box constraints (such as "L-BFGS-B") allowed us to specify an upper limit on the parameter d (dispersal rate), which was important because arbitrarily large dispersal rates were indistinguishable from one another (Fig. S3).

To further validate the performance on our model fitting machinery, we tested it against random data that we simulated from known underlying distributions. In short, we simulated the deterministic *lagged dispersal* model with known parameters (r=0.2 day^{-1}, K=100 vectors host^{-1}, d=0.2 day^{-1}, β_{VH}=0.005 hosts vector^{-1} day^{-1}, β_{HV}=0.68 arenas host^{-1} day^{-1}) and then simulated random data around it that matched the structure of the actual data collected in the experiment (i.e., replication, times sampled, etc.). We simulated infection data as a Bernoulli process with probability of infection equal to infection prevalence in the deterministic model ($\frac{I_2}{S_2+I_2}$), and we simulated aphid abundance data as a negative binomial process with a mean equal to the abundance predicted by the deterministic model ($V_2 + W_2$) and a reasonable degree of overdispersion (θ=0.3). We simulated 100 unique datasets and tested our model fitting machinery on each one. We found that the model fitting machinery successfully estimated the underlying parameters used to generate the simulated data with a high degree of precision (Fig. S5: r=0.2 day^{-1}, K=100 vectors host^{-1}, d=0.2 day^{-1}, β_{VH}=0.005 hosts vector^{-1} day^{-1}, θ=0.3).

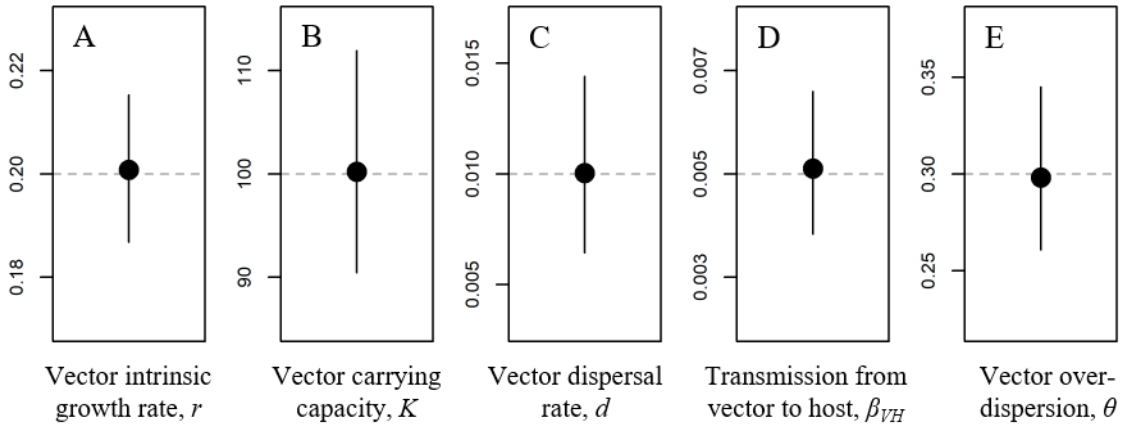

Figure S5. *Model fitting machinery performs well on simulated data.* Dashed gray lines show underlying parameters used to simulate data. Black circles show mean parameters as estimated by the model fitting machery along with 95% confidence intervals.

All three models fit to the experimental arenas

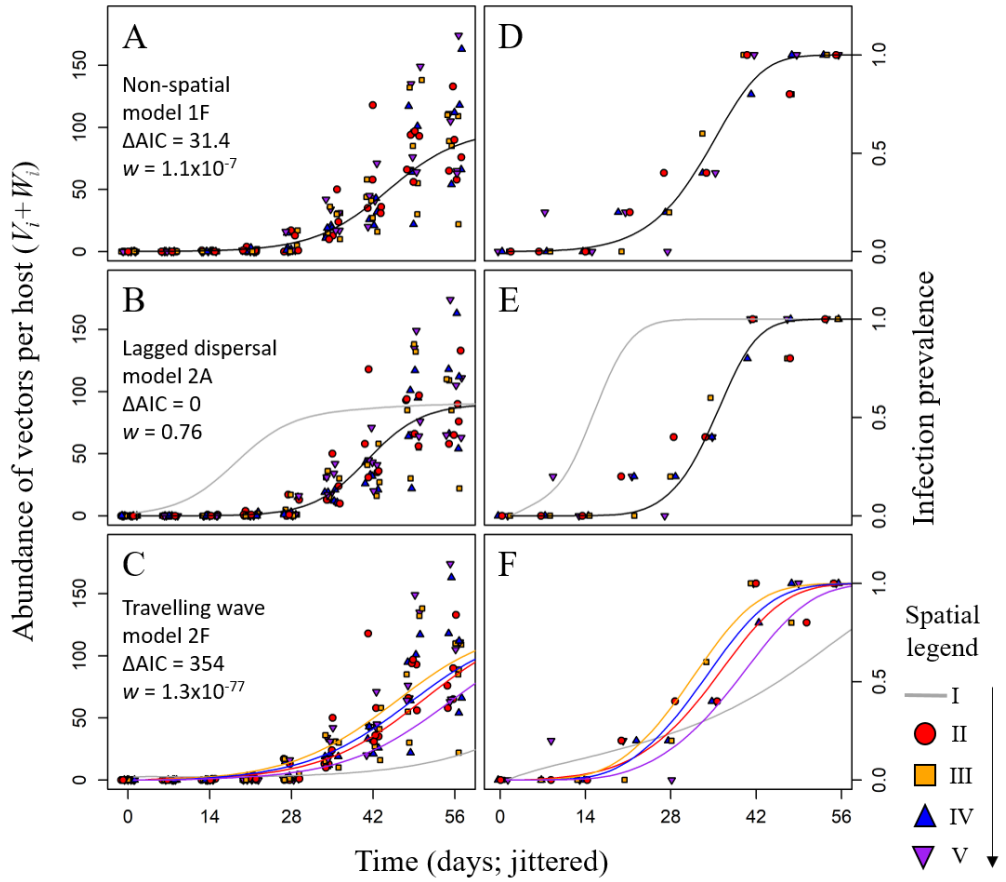

Figure S6. *All three models fit to experimental data.* The main text displays the best overall model fit to all experimental treatments (Fig. 3) and reports AIC-based results of the model competition (Table 3). Here we show the simplified *non-spatial* model (model 1F), the best overall *lagged dispersal* model (model 2A), and the analogous *travelling wave* model (model 2F), all fit to one experimental treatment (-R, +D: low resource supply, with disease). The lagged *dispersal model* provided the best overall fit to both B) aphid abundance and E) plant infections. A & D) The simplified *non-spatial* model fit decently well, but was inferior to *lagged dispersal* (ΔAIC = 31.4). C & F) The *travelling wave* model fit very poorly in comparison (ΔAIC = 354). Fitted parameters for each model shown here are listed in Table S2.

Fitted parameters

Table S2. *Fitted parameters for vector demography, dispersal, and transmission from the simplified non-spatial model (model 1F), the best overall lagged dispersal model (model 2A), and the analogous travelling wave model (model 2F). Models fitted to data are displayed in Figs. 3 & S6.*

Vector trait	Treatment	Simplified *non-spatial* (model 1F)	Best *lagged dispersal* (model 2A)	Analogous *travelling wave* (model 2F)
population growth rate, $\boldsymbol{r}$ (day^{-1})	-R, -D	0.237	0.246	0.171
	-R, +D	0.158	0.212	0.110
	+R, -D	0.216	0.216	0.158
	+R, +D	0.180	0.180	0.126
carrying capacity, $\boldsymbol{K}$ (vectors $host^{-1}$)	-R (+/- D)	98.6	90.3	125.8
	+R (+/- D)	156.9	156.9	204.4
dispersal rate, $\boldsymbol{d}$ (day^{-1})	-R, -D	-	0.141	0.095
	-R, +D	-	0.0112	0.444
	+R, -D	-	0.486	0.088
	+R, +D	-	0.5	0.437
transmission coefficient, $\boldsymbol{\beta_{VH}}$ (hosts $vector^{-1}$ day^{-1})	all	0.00539	0.00589	0.00452
vector overdispersion, $\boldsymbol{\theta}$	all	0.296	0.278	0.583

Likelihood surfaces of parameters from the best overall model

We inspected likelihood surfaces to investigate how the model fitting arrived at the best 'compromise' of parameters *r*, *K*, and *d* (Fig. S7). These likelihood surfaces highlight potential statistical associations that can arise when fitting multiple parameters. For example, we were concerned that higher estimates of *K* may have forced compensatory lower estimates of *r* in the fertilized arenas. If such an association existed, the likelihood surface in *r* x *K* space could show a 'ridge' with likelihood peaking along a negative correlation between *r* and *K*. This type of surface would indicate that similarly high levels of likelihood were reached with either lower *r* and higher *K*, or higher *r* and lower *K*. In contrast, a 'bullseye' would indicate a single peak in

the likelihood surface. We found 'bullseye' likelihood peaks in *r* x *K* space, but we found some evidence of 'ridges' in *r* x *d* space. Specifically, in the unfertilized arenas, higher estimates of *r* could be compensated by lower estimates of *d* (and vice versa), without sacrificing much likelihood. However, the range of reasonable values for both *r* and *d* still varied substantially among treatments (more than variation along the 'ridges' in the likelihood surfaces). Therefore, the effects that we detected of resources and disease on *r*, *K*, and *d* (Fig. 4 in the main text) seem robust to these statistical associations among parameter estimates.

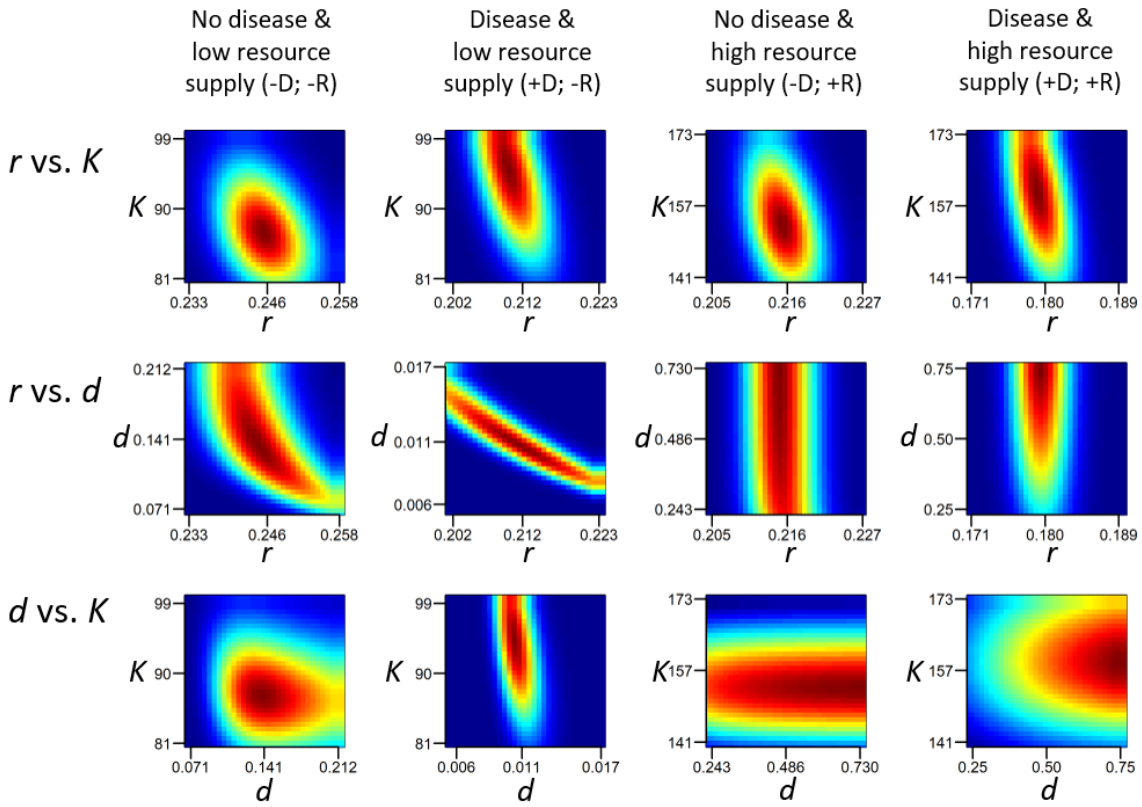

Figure S7. *Likelihood surfaces.* Columns show different treatments of the experiment; rows show each pairwise combination of the parameters *r*, *K*, and *d*. Colors show likelihood calculated with eq. S15 and the best overall model (model 2A; red=higher; blue=lower). Gradients of each

parameter are centered at their estimate (Table S2) and extend 5% (for *r*), 10% (for *K*), or 50% (for *d*) in either direction. All other parameters are set to their fitted values in the best overall model (Table S2; model 2A). **Top row:** Likelihood surfaces showed robust single peaks for combinations of *r* and *K*. **Middle row:** Unfertilized arenas showed negative associations between *r* and *d*, but the range for both parameters is small relative to the differences among treatments (note axis scaling; Fig. 5 in the main text). In fertilized arenas, the likelihood surface became a 'smear' as *d* increased, because dynamics on donor and receiver hosts became arbitrarily similar (Fig. S3). **Bottom row:** Unfertilized arenas showed robust single peaks for combinations of *d* and *K*. Fertilized arenas showed similar 'smears' as *d* increased.

REFERENCES

Carpenter, B., M. D. Hoffman, M. Brubaker, D. Lee, P. Li, and M. Betancourt. 2015. The Stan math library: Reverse-mode automatic differentiation in C++. arXiv preprint arXiv:1509.07164.

Gray, S. M. 2008. Aphid transmission of plant viruses. Current Protocols in Microbiology **10**:16B.11.11-16B.11.10.

Hoagland, D. R., and D. I. Arnon. 1950. The water-culture method for growing plants without soil. Circular. California Agricultural Experiment Station **347**:32 pp.

Ver Hoef, J. M., and P. L. Boveng. 2007. Quasi-poisson vs. negative binomial regression: How should we model overdispersed count data? Ecology **88**:2766-2772.